2024 年 3 月 21 日

令和 5 年度　国際研究交流推進事業 報告書

報告者氏名　岡村　秀雄
事業名　　国際研究交流推進事業
期間　　2023 年 4 月～2026 年 3 月

研究課題名　インドネシアと日本における水環境に残留する化学物質の生態リスク研究および気候変動がおこす水力学の変化の影響

課題① インドネシアと日本における水環境に残留する化学物質の生態リスク研究

（野村美帆、岡村秀雄、堀江好文）

研究概要

プラスチック汚染は最も深刻な環境問題の一つである。プラスチック製品には用途に合わせて様々な添加剤が含まれているが、低分子量である添加剤は高分子のプラスチックと化学的に結合していないため環境中で溶出する可能性があり、溶出した化学物質は水生生物の生育・生長に影響を及ぼすことが懸念される。添加剤の中でも可塑剤は最も使用量の多い添加剤の一つである。主な可塑剤としてフタル酸エステル類が広く使用されてきたが、生物に対して内分泌かく乱作用を持つ可能性があるため、日本、欧州、米国では現在 6 種類のフタル酸エステル類の使用が規制されている。フタル酸エステル類の規制に伴い、代替可塑剤として非フタル酸可塑剤が使用されているが、非フタル酸可塑剤の生態リスクに関する知見は少ない。そこで、本研究ではインドネシアと日本の海水や河川水、底泥中の非フタル酸可塑剤の生態リスクを評価することを目的として、5 種の非フタル酸可塑剤として Diisobutyl adipate (DIBA), Acetyl tributyl citrate (ATBC), Di-(2-ethylhexyl) adipate (DEHA), Di-(2-ethylhexyl) sebacate (DEHS), Trioctyl trimellitate (TOTM)を対象として環境中での動態の把握及び生態毒性を評価する。具体的な実験項目を以下に示す。本事業では主にインドネシア、ジョグジャカルタ特別州における河川水、河川底泥中の非フタル酸可塑剤の残留分析を行う。

(1) 水生生物に対する非フタル酸可塑剤の影響評価
(2) 非フタル酸可塑剤の生分解性・光分解性評価
(3) 大阪湾・ジョグジャカルタ（インドネシア）における非フタル酸可塑剤の環境残留の把握
(4) 土壌粒子への非フタル酸可塑剤の吸着性評価

研究成果と今後の計画

初年度は海水中の非フタル酸可塑剤の分析方法を確立し、大阪湾における海水・底泥中の非フタル酸可塑剤の環境残留分析を実施した。その結果、非フタル酸可塑剤はろ過海水よりも底泥中に高濃度で残留していることが明らかになった[1]。

2023 年 11 月 14 日～11 月 27 日にジョグジャカルタに滞在し、ガジャマダ大学(UGM)を訪問した。滞在期間中は UGM の指導教員と研究計画について議論し、UGM の設備を確認し、採取した河川水・河川底泥試料を UGM の既存の設備を用いて処理・分析できるかどうかを検討した。また、現地の河川の様子を下流から上流にかけて調査し、水・泥試料をサンプリング可能であるかを確認した。

来年度は河川水・河川底泥を採取し、処理後の試料を日本に持ち帰った後、試料中の非フタル酸可塑剤濃度を測定する。異なる季節に試料を採取することで環境中に残留する非フタル酸可塑剤濃度の季節変動を把握するとともに、大阪湾における非フタル酸可塑剤残留濃度と比較することで日本とインドネシアでの残留状況の違いを明らかにする。来年度は計 3 回の渡航を計画しており、1 回目は 2024 年 4 月 25 日～7 月 2 日の予定で先方と調整している。

研究成果

[1] M. Nomura, H. Okamura, Y. Horie, M. P. Hadi, A. P. Nugroho, B. R. Ramaswamy, H. Harino, T. Nakano, 2024. Residues of non-phthalate plasticizers in seawater and sediments from Osaka Bay, Japan, Marine Pollution Bulletin, 199, DOI: 10.1016/j.marpolbul.2023.115947

課題② Volcanic Dome Hazards and subsequent disaster risks (comparison of Unzen and Merapi Volcanoes)
（大海陸人、クリストファーゴメス）

研究概要

R. Daikai begun his research career at the SABO laboratory in collaboration with two researchers from UGM (Universitas Gadja Madah) and UMS (Universitas Muhammadiyah Surakarta) in Indonesia [1].
After publishing his first international paper, he continued to Master, which he is finishing in March 2024, obtaining the department best presentation award. From April, he will begin his PhD in co-tutelle with UGM University, and the present collaboration program allowed him to go and meet his future supervision team.

He also went to UMS (Universitas Muhammadiyah Surakarta), where he gave a lecture on the new bulk-sediment density method based on SfM-MVS photogrammetry, which he is presently perfecting (paper in preparation for the journal of the Sabou-gakkai).

Both Unzen and Merapi have been considered sister volcanoes, because of the manner the domes collapse into block and ash pyroclastic density-currents (previously named pyroclastic flows).
Although Unzen Volcano is presenting a dome that is moving as a landslide by a few mm a year (the Master thesis of Daikai Rikuto, with a submission in preparation for the Journal of Volcanology and Geothermal Research), the Merapi Volcano, which still has an active feeding column is displaying further explosive activity, such as phreatomagmatic explosion.

Leveraging the MOU we signed between the faculty of Oceanology and UGM, and the University of Paris 1 Sorbonne in France, the team studied the explosions of the dome of Mt. Merapi [2], and we were able to make further observations during the field trip that lasted from the 14th to the 17th November 2023.

研究成果

[1] R. Daikai, C. Gomez, B. Bradak, Saputra, A., D. Sri Hadmoko. 2022. Predisposition Factor of Safety of Landslide Dams from Typhoon Talas, Kii peninsula, Japan. Forum Geografi 36, 2,
doi: 10.23917/forgeo.v36i2.20668

[2] C. Gomez, M.A., Setiawan, N. Listyaningrum, S. B. Wibowo, D.S. Hadmoko, W. Suryanto, H. Darmawan, B. Bradak, R. Daikai, S. Sunardi, Y. Prasetyo, A. J.Astari, L. Lukman, I.W., Nurani, M. Dede, I., Suhendro, F. Lavigne, M.N. Malawani. 2022. LiDAR and UAV SfM-MVS of Merapi Volcanic Dome and Crater Rim Change from 2012 to 2014, Remote Sensing 14, 5193, https://doi.org/10.3390/rs14205193

添付資料

上記論文3編の pdf ファイル

FORUM GEOGRAFI
ISSN: 0852-0682 | E-ISSN: 2460-3945
HTTPS://JOURNALS.UMS.AC.ID/INDEX.PHP/FG/

Predisposition Factor of Safety of Landslide Dams from Typhoon Talas, Kii Peninsula, Japan

Rikuto Daikai [1, *], Christopher Gomez [1], Balazs Bradak [1], Aditya Saputra [2], Danang Sri Hadmoko [3]

[1] Graduate School of Oceanology, Sediment Hazards and Disaster Risk Laboratory/ Kobe University, Kobe, Japan
[2] Department of Geography, Universitas Muhammadiyah Surakarta, Surakarta, Indonesia
[3] Department of Environmental Geography, Faculty of Geography, Universitas Gadjah Mada, Indonesia

[*)] Correspondance : rikuto.d221@gmail.com

Citation:
Daikai, R., Gomez, C., Bradak, B., Saputra, A., & Hadmoko, D.S. (2022) Predisposition Factor of Safety of Landslide Dams from Typhoon Talas, Kii Peninsula, Japan. Forum Geografi. Vol. 36, No. 2.

Article history:
Received: 4 July 2022
Accepted: 29 December 2022
Published: 28 December 2022

Abstract

Landslide dams are less frequent than other landslides, and their very existence is often very-much short-lived, because the temporary dam tends to collapse rapidly. Because of the resulting lack of evidences, there has been less research done on this topic, although the potential catastrophe they can be at the origin of needs assessment. For this purpose, the present contribution aims at differentiating landslides that trigger dams against those that do not inside a group of valleys of the Kii peninsula in Japan, where landslides occurred after the typhoon Talas in 2011. Using topographic map before the event and LiDAR data in its aftermath, the authors have calculated the factor of safety (FS) of different landslides in the same valleys, comparing the data of landslides that created dams against those that did not. The results show that landslides that triggered dams seemed to have a higher FS than those that did not. The authors suggest that it is because larger landslides are needed and thus appear more stable, but also because at the location where the slopes are stable, the riverbed can incise further instead of growing horizontally, and thus the sediments damming the channel have more chances to block it (as it is narrow) and stop the river from flowing.

Keywords: landslide predisposition facts, landslide dams.

1. Introduction

Landslides (Hadmoko and di Mauro, 2012) and landslides' dams are a major threat across mountainous regions of the world, with the potential of sudden dam-breach, which in turn have the potential to lead to downstream floods. Moreover, recreational mountaineering and climate change have increased the disaster risk due to mass movements (Purdie *et al.*, 2015).

The largest contemporary landslide dam on Earth is the Usoi dam, produced in 1911 in Tajikistan, with a lake as deep as 505 m. Other smaller-size landslides can be found in most countries with mountainous areas: in Turkey, the Tortum dam is 180 million m3 dam, impounding a 6.77 km2 surface lake (Duman, 2009). Across the world, Costa and Schuster (1991) recorded 463 landslide dams, and more recently Korup (2002) recorded more than 130 for New Zealand only and Yan (2006) found 388 for China alone, suggesting that the data first provided are very conservative. More recently, Peng and Zhang (2012) compiled a database with 1,239 landslide dams, demonstrating the difficulty of working with landslide dams, because they are often temporary features, which are often drained when possible. Peng and Zhang (2012) have demonstrated that 87% of landslide dam fails within one year, while 71% within 1 month and a bit more than half within a week, and that the failure occurs by either overtopping (90%), piping (8%), and slope failure (1%). Interestingly, they also demonstrated that this distribution does not compare well with the man-made earth and rockfill dams. Consequently, morphological indices of valley dams (Stefanelli *et al.*, 2016) and statistical approaches (Shen *et al.*, 2020) are being employed to improve scientific understanding of the longevity of landslide dams and when they are most likely to break.

Because of the difficulties, Science still faces with fully physical simulations for prediction of frequency and runout (e.g. Huang *et al.*, 2015; Cama *et al.*, 2015), remote sensing (Gomez and Purdie, 2016; Lissak *et al.*, 2020) combined with statistical and geostatistical methods has been widely used (Saputra *et al.*, 2015). These methods have especially led to empirical predictors relying on geometric factors (e.g., volume, area, runout, and distance to river, H/L ratio, type, and lithology) and the statistical relations between these parameters (Fan *et al.*, 2014). The relation between the translated volume of material and the deposition extend has been found to be a power law relating the area of the landslide A [m2] to the volume V [m3], so that: V = 0.316A1.361, with a R2 of 0.906 (Chen *et al.*, 2014). In Hokkaido (North Japan), the relation between the width (W) and the length of the deposit (L) also showed that for earthquake-triggered landslides in the immediate aftermath of a typhoon. The relation was almost scale-invariant with L=2.2492W1.0296 (R2=0.89). Moreover, in Hokkaido the runout was exceptionally long (Gomez and Hotta, 2021), with a H/L ratio between 0.15 and 0.5 for relatively small landslides. This H/L

ratio - or Fahrboschung - was calculated to be F=0.3521-9*10EXP-06D (Gomez and Hotta, 2021). By comparison, the Naga landslide (Catane *et al.*, 2019), and the Zhaotong rock avalanche of 1991 (Xing *et al.*, 2020) show Fahrboschung of 0.17 to 0.25, which at equal volume in Hokkaido would lead to a Fahrboschung of 0.028. It shows that in between locations and events, there are great disparities, but at the same time the research corpus also suggests that for a single type of events in homogeneous valleys and lithologies, comparable geometric relations can also be expected.

To these inherent difficulties, landslide dams add further challenges to their predicting, as it is the case for secondary- and multi-hazards (Saputra *et al.*, 2021). Indeed, in a geologically "homogeneous region", only a small proportion will block valleys and generate impoundments. For instance, out of the approximately 30,000 landslides generated by the 12 May 2008 Sichuan Earthquake, only 257 blocked rivers to form impounded lakes (Cui *et al*., 2009; Peng and Zhang, 2012). Moreover, landslide dams generated by rainfall-induced landslides tend to collapse in 82% of cases, while earthquake-induced landslides tend to be more stable (57% collapse) under the pressure of the impounded water (Kuo *et al.*, 2011), further emphasizing the difficulty in predicting potential for impoundments and downstream floods.

In the light of this research body, which suggests that in homogeneous terrain, and for a homogeneous triggering event, the variability is site specific and eventually linked to the morphology of the slope, the objective of this work has been to test whether the factor of safety (Fs) could be used as a factor to determine whether a landslide could turn into a dam or not. Such work would then allow for pre-event assessment of the slopes from high-resolution topographic data, prior to further engineering invasive investigation.

2. Research Method

To reach the present objective, the research was conducted at the Kii peninsula, located to the south-west of Honshu Island, Japan (Figure 1), where a set of landslides have occurred following the landfall of typhoon 12 or Typhoon Talas, on September 3rd, 2011 (Figure 2). The local topography is characterized by elevation not exceeding 1,500 meters, but with slopes commanding topographic gradients of 500 m to 800 m locally, with gravel-bed rivers resulting for the tectonically active area. Erosion is an important shaping factor of these reliefs as they are cut from shale with blocks of chert and greenstones alternating with sandstones, dating back to 80~90 million years. This material was generated as part of the Ryujin accretionary prism, created by the subduction of the tectonic plates, and dated to be Middle Miocene in igneous rocks with signs of remobilization during the late Maastrichtian based on U-Pb dating (Hoshi *et al*., 2022).

This typhoon was the second catastrophic event after the 1889 typhoon, which brought 1000 mm of rainfall to the Kii Peninsula (Kharismalatri *et al*., 2017). The geology belongs to the Miyama Formation of the Hidakagawa Group, which is part of the Chalk Shimanto Belt and is composed mainly of chert, greenstones, and alternating sandstone and shale (Kinoshita *et al.*, 2013).

Using 8 landslides, triggered by the typhoon 12 (or Typhoon Talas), four of which became landslide dams (Figure 3), the authors reconstructed the topography prior to the landslide using the 1989 topographic maps 1/25,000 and the new topographic profiles in the center of the landslide scar from LiDAR data, in order to measure the depth of the slide by subtracting one from the other. The alignment of both dataset was performed using the open-source software Cloud-Compare and QGIS, based on 86 and 99 control points for the two map tiles used in the present study. In both cases, the alignment error was 3.24-11 and 9.14-12 and deemed to have no significant effect on the results. The 1989 map were used as a confirmation that the local slope was in continuation to the surrounding ones that did not collapse. This way the edge of the landslide measured from the LiDAR data were interpolated to the missing areas from which the pre-landslide topographic profile was generated (the data are provided in appendix as a csv file).

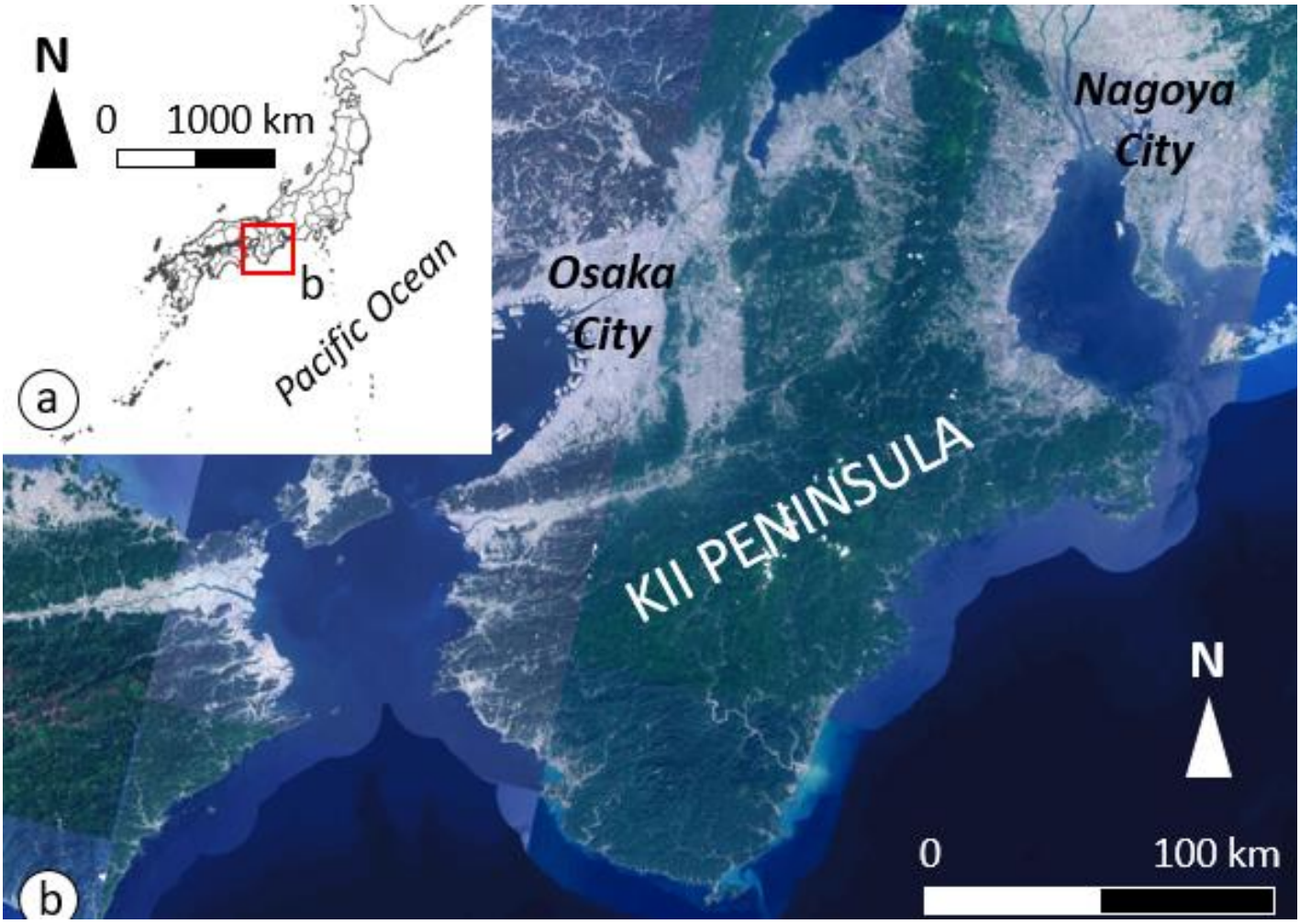

Figure 1. Regional Map of the research area (a) map of Japan with the survey region squared in red, (b) Kii Peninsula located in between Osaka City and Nagoya City.

In order to link the landslide to predisposition factors of stability, the authors have used the infinite slope model, for which the unit density of material was tested at 20 kN/m3 (γ) was used as a simplification of the local material. The stability of slopes using the infinite slope method is based on the shear strength equation:

$$\tau_c = C' + \sigma' \tan \varphi' \qquad (1)$$

Where τ_c is the shear strength, C^' is is the cohesion, σ^' is the normal stress on the potential failure surface and φ' is the angle of friction. If we simplify the concept by omitting the pore pressure and water intake to compare slopes using the factor of safety (F_s), the equation can be reduced to:

$$F_s = \frac{C\prime}{\gamma H \cos^2 \beta \tan \beta} + \frac{\tan \varphi\prime}{\tan \beta} \qquad (2)$$

Where H is the depth at which the failure occurs, and β is the slope angle of the failure plane. This equation was computed in the open-source software Hyrcan, using the method of slice (http://www.geowizard.org/download_hyrcan.html). Iteratively, Hyrcan tests the potential failure planes at different depths. The highest probability of failure corresponds to the "lowest" factor of safety, which once calculated was compared to the landslide failure plane, so that the authors

could define whether – or not – the location of the simulated failure plane corresponded to the actual failure plane following the September 2011 rainfall landslides.

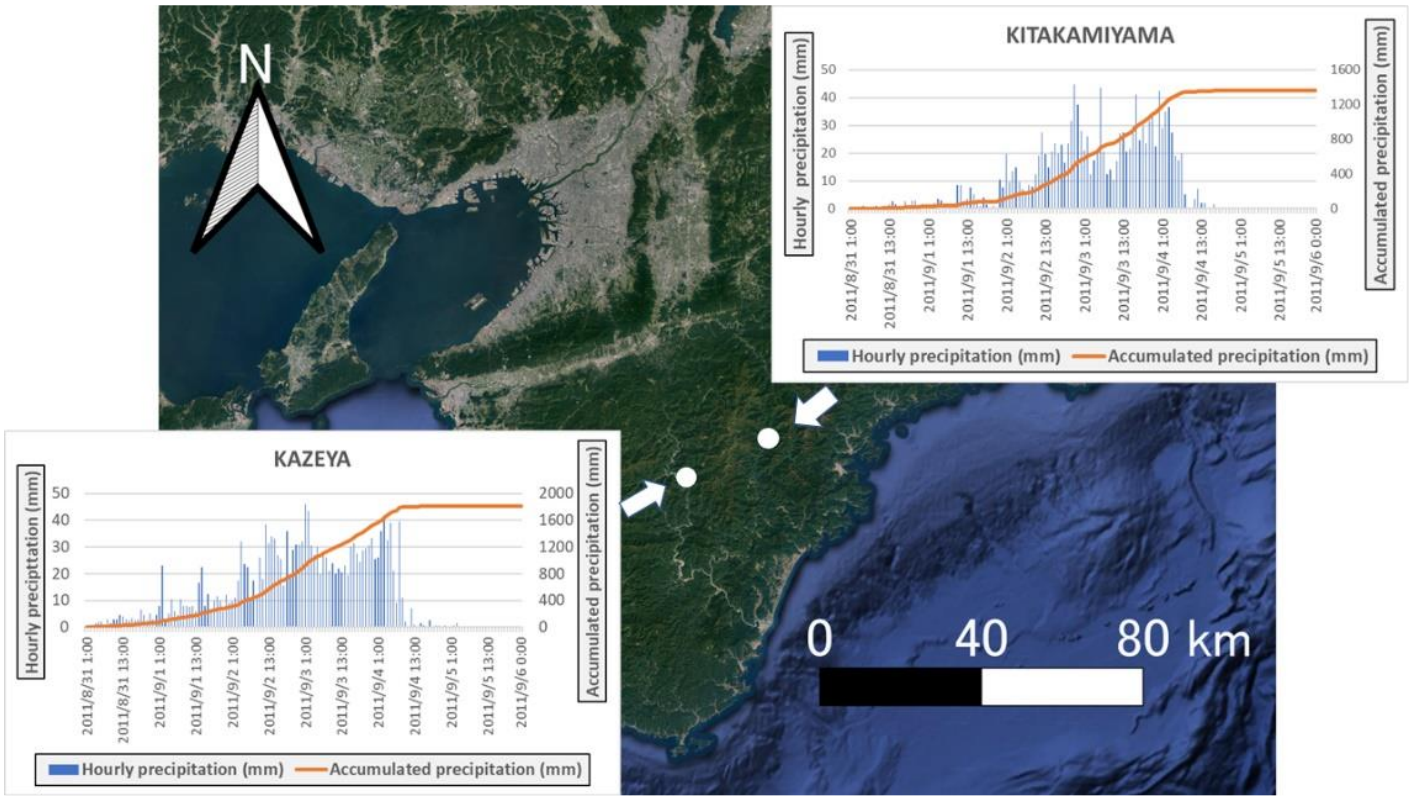

Figure 2. Rainfall Record of the 2011 Talas Typhoon (Typhoon 12) over the Kii Peninsula.

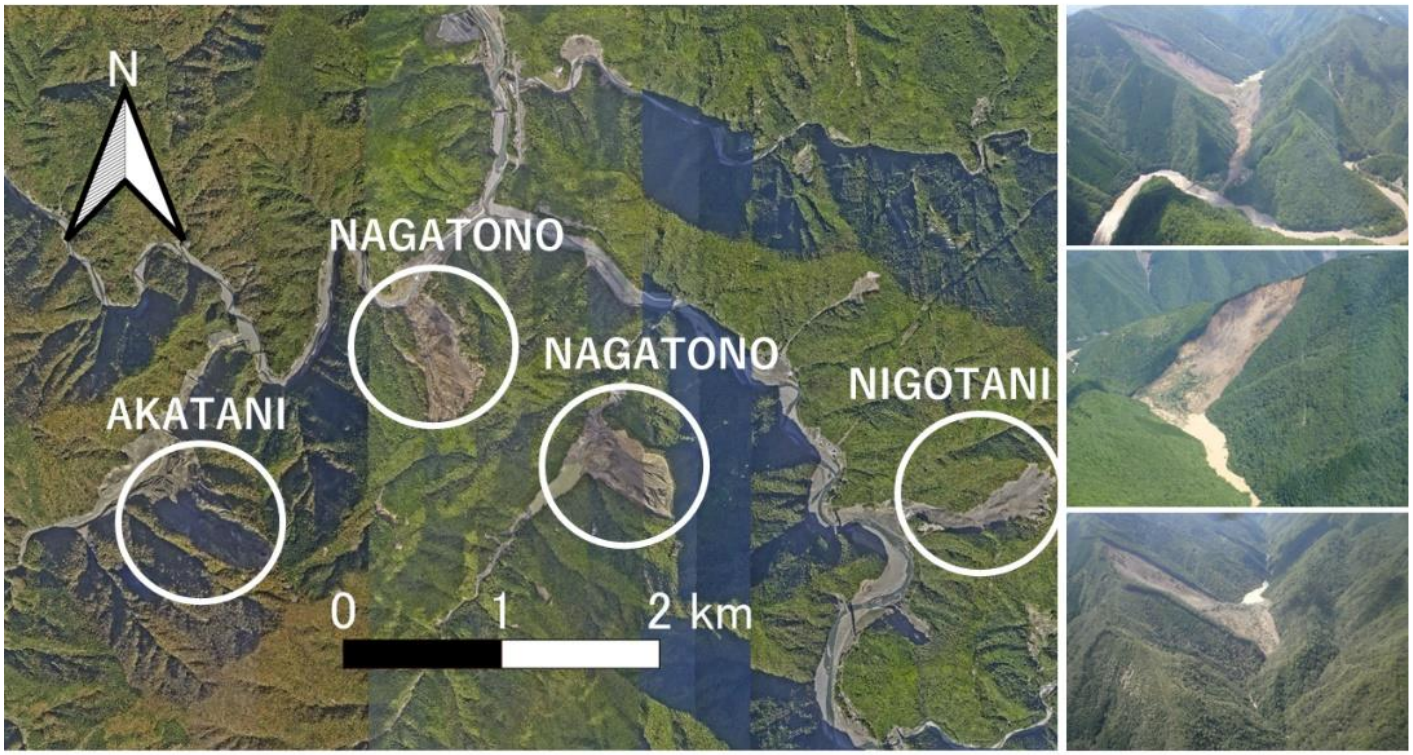

Figure 3. Aerial oblique photographs of the four studied landslides triggered by typhoon 12 in Nara prefecture, on the Kii Peninsula (source: MLIT).

3. Results and Discussion

3.1. Results

The 8 simulated landslides show depths (H) varying between 0.017 m and 83.160 m. The deepest simulated landslide found a depth of 83.160 m at AKATANI② location. The actual landslide depths varied between -0.073 m and 76.900 m, and the local discrepancy vary from 0 m to 44.696 m locally, with an underestimation of the sliding plane at AKATANI① landslide (Figure 4). At AKATANI and NAGATONO landslide, the lower part of the sliding plane does not correspond to the simulation, because accumulation occurred in the valley, and such accumulation could not be taken into account.

For the landslides that did not trigger a landslide dam, the depths varying between 0.009 m and 45.120 m. The deepest simulated landslide found a depth of 45.120 m at NIGOTANI① location. The actual landslide depths varied between -4.748 m and 58.500 m, and the local discrepancy vary from 0 m to 35.398 m locally, with an underestimation of the sliding plane at NIGOTANI② landslide (Figure 5).

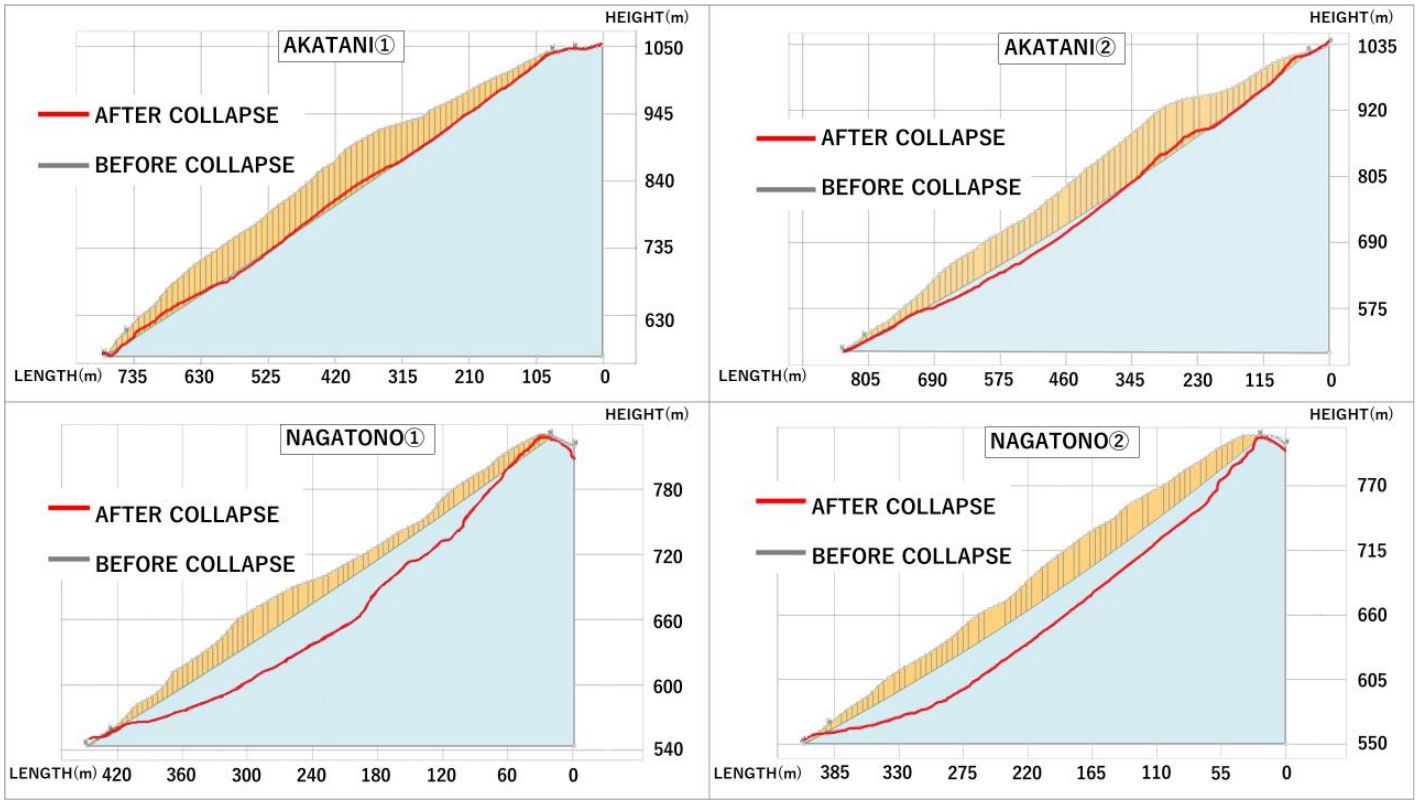

Figure 4. Profiles of the landslides that triggered landslide dams, with the simulated landslide and the actual sliding plane. The orange-coloured slices reveal the slicing method used to solve the factor of safety on the slope.

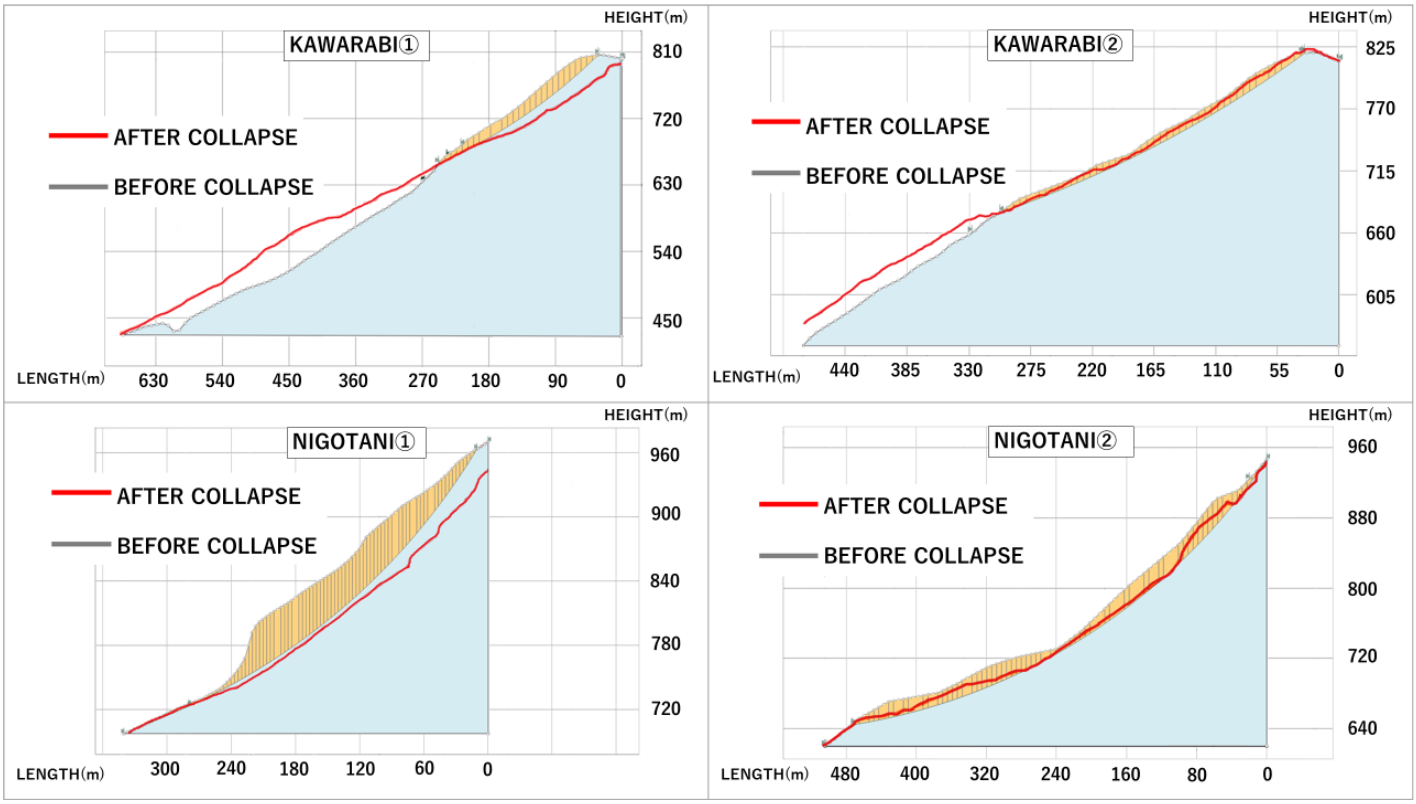

Figure 5. Landslide profiles for which landslide dams did not occur, comparing the simulated landslide against the actual landslide.

The differentiation in typical depth and sheer size of the landslides that triggered landslide dams compared to the normal landslide also exists when comparing the factor of safety for all of them (Table 1). Indeed, the factor of safety of the landslides that triggered landslide dams are comprised between 0.896 and 1.1, while those for landslides that did not trigger landslides, the FS is lower and comprised between 0.692 and 0.877. Consequently, predicting the potential of landslide dams based on soil mechanics and equilibrium approach can be challenging, as the method is not best suited to predict those.

Table 1. Factor of safety of the 8 different landslides. The landslides that triggered landslide dams have a higher safety factor than those that did not trigger landslide dams.

Location	AKATANI①	AKATANI②	NAGATONO①	NAGATONO②
FS	0.859	0.896	0.877	0.852
Location	KAWARABI①	KAWARABI②	NIGOTANI①	NIGOTANI②
Fs	0.811	1.1	0.692	1.02

3.2. Discussion

The present investigation of the predisposition factors for a selection of 8 landslides for which data were accessible, shows that the landslides that trigger temporary dams in river are eventually larger than their other counterparts, but also that the factor of safety is actually higher. The interpretation of the results suggests that landslides that occur less often are then eventually able to remobilize a greater amount of material, but also that the valley floor might play an important control role as well. Indeed, if sediments are continuously supplied to the valley floor, a widening and an adaptation to this situation occurs in the river network. To the contrary, a zone with no or less sediment supply will result in more vertical erosion and a potentially narrower channel, which in turn, during rare events will tend to be more prone to be filled up and to block the valley. Such characteristics, as well as road cuts are both well-known triggering factors of landslides (Ling and Chigira, 2020).

As Cui et al. (2009) expressed, only a few percent of the triggered landslides generate landslide dams. The present finding is in line with these existing findings, because – based on this limited study – their Fs is slightly higher. In other words, slopes that are less stable and prone to progressive erosion and small-scale mass movements are despite of their appearance not the most dangerous, they are most likely to not trigger a large-scale event. This is however not always the case as series of large-scale landslides can also occur and temporarily block rivers (Gomez *et al.*, 2020).

Hadmoko *et al.* (2010) discusses that qualitative, semi-quantitative and quantitative methods have been developed to measure hazards and disaster risks, and so using a broad range of datasets that can characterize the landslides. This logic is based on the concept that previous landslides can be used as a base to characterize future events. This broad concept is verified in the present case as well for landslides that are "dam-genic", because the FS – which is an expression of geometric parameters of the slope in absence of rainfalls - have shown to be of a higher Fs compared to landslides that are not dam-genic. This in turn signifies that, within a certain level, there are geometric parameters - besides the influence of rainfalls - that are sufficient to differentiate large vs small more regular landslides for the Kii peninsula.

The comparison provided in the present contribution however, is based on one single rainfall events, which, if one disregards the spatial variability of rainfall, and so in one single set of geological units. But this realm may not hold in complex and very differentiated geological settings or in the case when rainfalls or earthquake acceleration vary spatially. At present, understanding how one factor play over another one is often difficult, and scientists have often to resort using the simple events in the dataset (e.g., extracting the mass movements with deposits that did not mix with other deposits: Gomez and Hotta, 2021), like it is the case here, but there is still further work to be done on the role of multiple factors together.

4. Conclusion

In conclusion, we have proven that, before a rainfall event occurs, it was possible for a homogeneous catchment to predict landslides that will be more prone to trigger natural dams against those that have less probability to trigger one. Landslides that can be the source of landslide dams are of larger amplitude and are more difficult to predict, because of their higher Fs values. The investigation found that landslides triggering temporary dams in rivers tend to be larger but have a higher factor of safety, while slopes that are less stable and prone to small-scale movements are not necessarily the most dangerous. The study suggests that previous landslides can be used to characterize future events, particularly for "dam-genic" landslides, but further work is needed to understand the role of multiple factors together in complex geological settings.

Acknowledgements

The present research was part of the Graduate Thesis of Mr. Daikai Rikuto, obtained at Kobe University, Department of Oceanology, Laboratory of Sediment Hazard and Disaster Risk. Our thanks go to the Sabo Office of Wakayama Prefecture, which supported the presentation of the preliminary data at the Sabo-gakkai Taikai in Miyazaki Prefecture in 2022.

Author Contributions

Conceptualization: Rikuto Daikai, Christopher Gomez, Balazs Bradak, Aditya Saputra, Danang Sri Hadmoko; **methodology**: Rikuto Daikai, Christopher Gomez, Balazs Bradak, Aditya Saputra, Danang Sri Hadmoko; **investigation**: Rikuto Daikai, Christopher Gomez, Balazs Bradak, Aditya Saputra, Danang Sri Hadmoko; **writing—original draft preparation**: Rikuto Daikai, Christopher Gomez, Balazs Bradak, Aditya Saputra, Danang Sri Hadmoko; **writing—review and editing**: Rikuto Daikai, Christopher Gomez, Balazs Bradak, Aditya Saputra, Danang Sri Hadmoko; **visualization**: Rikuto Daikai, Christopher Gomez, Balazs Bradak, Aditya Saputra, Danang Sri Hadmoko. All authors have read and agreed to the published version of the manuscript.

References

Cama, M., Lombardo, L., Conoscenti, C., Agnesi, V., Rotigliano, E. (2015) Predicting storm-triggered debris flow events: application to the 2009 Ionian Peloritan disaster (Sicily, Italy). Naturall Hazards Earth System Sciences 15, pp. 1789-1806.

Catane, S., Vercruz, N., Flora, J., Go, C., Enrera, R., Santos, E. (2019) Mechanism of a low-angle translational block slide: Evidence from the September 2018 Naga Landslide, Philippines. Landslides 16, pp. 1709-1719.

Chen, K.-T., Kuo, Y.-S., Shieh, C.-L. (2014) Rapid Geometry Analysis for Earthquake-induced and Rainfall-induced Landslide Dams in Taiwan. Journal of Mountain Sciences Vol. 11, pp. 360-370.

Costa, J.E., Schuster, R.L. (1991) Documented historical landslide dam found around the world. US Geological Survey Open-File Report Vol. 91, 486p.

Cui, P., Zhu, Y.U., Han, Y.S., Chen, X.Q., Zhuang, J.Q. (2009) The 12 May Wenchuan earthquake-induced landslide lakes: distribution and preliminary risk evaluation. Landslides Vol.6, pp.209-223.

Duman, (2009) The largest landslide dam in Turkey: Tortum landslide. Engineering Geology Vol. 104, pp. 66-79.

Fan, X., Rossiter, D.G., van Westen, C.J. van, Xu, Q., Gorum, T. (2014) Empirical prediction of coseismic landslide dam formation. Earth Surface Processes and Landforms Vol. 39, pp. 1913-1926.

Gomez, C., Purdie, H. (2016) UAV-based photogrammetry and geocomputing for hazards and disaster risk monitoring – a review. Geoenvironmental Disasters 3, 1-11.

Gomez, C., Hotta, N. (2021) Deposits' Morphology of the 2018 Hokkaido Iburi-Tobu Earthquake Mass Movements from LiDAR and Aerial Photographs. Remote Sensing Vol. 13-3421, https://doi.org/10.3390/rs13173421

Gomez, C., Allouis, T., Lissak, C., Hotta, N., Shinohara, Y., Hadmoko, D.S., Vilimek, V., Wassmer, P., Lavigne, F., Setiawan, A., Sartohadi, J., Saputra, A., Rahardianto, T. (2020) High-Resolution Point-Cloud for Landslides in the 21st Century: From Data Acquisition to New Processing Concepts. In World Landslide Forum: Understanding and Reducing Landslide Disaster Risk, pp. 199-213.

Hadmoko, D.S., Lavigne, F., Sartohadi, J., Hadi, P., Winaryo. (2010) Landslide hazard and risk assessment and their application in risk management and landuse planning in eastern flank of Menoreh Mountains, Yogyakarta Province, Indonesia. Natural Hazards Vol. 54, pp. 623-642.

Hadmoko, D.S., Di Mauro S.E. (2012) Landslide and other Mass Movements. In The Routledge Handbook of Hazards and Disaster Risk Reduction (Eds. Wisner et al.). 13p.

Hoshi, H., Kawakami, Y., Iwano, H., Danhara, T. (2022) Zircon U-Pb and fission-track ages of felsic tuff from the Ryujin Complex in the Shimanto Accretionary Prism on the eastern part of the Kii Peninsula, Japan. Journal of the Geological Society of Japan 128, pp. 229-237 (in Japanese).

Huang, J., Ju, N.P., Liao, Y.J., Liu, D.D. (2015) Determination of rainfall thresholds for shallow landslides by a probabilistic and empirical method. Natural Hazards Earth System Sciences 15, pp. 2715-2723.

Kharismalatri, H.S., Ishikawa, Y., Gomi, T., Shiraki, K., Wakahara, T. (2017) Collapsed material movement of deep-seated landslides caused by Typhoon Talas 2011 on the Kii Peninsula, Japan. International Journal of Erosion Control Engineering, Vol. 10, pp. 108–119.

Kinoshita, A., Ogawauchi Y., Mayumi, T., Shibasaki, T. (2013) Geological factors of deep-seated catastrophic landslide and physical and mechanical properties of its sliding layer triggered by the heavy rainfall associated with Typhoon Talas（T 1112）in Kii Peninsula. Journal of the Sand Prevention Society Vol. 66-3, pp.3-12.

Korup, O. (2002) Recent research on landslide dams – a literature review with special attention to New Zealand. Progress in Physical Geography Vol. 26, pp. 206-235.

Kuo, Y.-Y., Tsang, Y.-C., Chen, K.T., Shieh, C.-L. (2011) Analysis of Landslide Dam Geometries. Journal of Mountain Sciences Vol. 8, pp. 544-550.

Ling, S., Chigira, M. (2020) Characteristics and triggers of earthquake-induced landslides of pyroclastic fall deposits: An example from Hachinohe during the 1968 M7.9 tokachi-Oki earthquake, Japan. Engineering Geology 264, 105301, pp. 1-11.

Lissak, C., Bartsch, A., de Michele M., Gomez, C., Maquaire, O., Raucoules, D., Roulland, T. (2020) Remote Sensing for Assessing Landslides and Associated Hazards. Surveys in Geophysics 41, pp. 1-45.

Peng, M., Zhang, L.M. (2012) Breaching parameters of landslide dams. Landslides Vol. 9, pp. 13-31.

Purdie, H., Gomez, C., Espiner, S. (2015) Glacier recession and the changing rockfall hazard: Implications for glacier tourism. New Zealand Geographer 71, pp. 189-202.

Shen, D., Shi, Z., Peng, M., Zhang, L., Jiang, M. (2020) Longevity analysis of landslide dams. Landslides Vol. 17, pp. 1797-1821.

Stefanelli, C.T., Segoni, S., Casagli, N., Catani, F. (2016) Geomorphic indexing of landslide dams evolution. Engineering Geology Vol. 208, pp. 1-10.

Saputra, A., Sartohadi, J., Sri Hadmoko, D., Gomez, C. (2015) Geospatial Assessment of Coseismic Landslides in Baturagung Area. Forum Geografi 29, 99-113.

Saputra, A., Gomez, C., Delikostidis, I., Zawar-Reza, P., Hadmoko, D.S., Sartohadi, J. (2021) Preliminary identification of earthquake triggered multi-hazard and risk in Pleret sub-district (Yogyakarta, Indonesia). Geo-spatial Information Science 24, 256-278.

Xing, A., Wang, G., Yin, Y., Tang, C., Xu, Z., Li, W. (2016) Investigation and dynamic analysis of a catastrophic rock avalanche on September 23, 1991, Zhaotong, China. Landslides 13, pp. 1035-1047.

Yan, R. (2006) Secondary disaster and environmental effect of landsllides and collapsed dams in the upper reaches of Minjiang River. Master Thesis, Sichuan University, 143 p. (in Chinese).

remote sensing

MDPI

Article

LiDAR and UAV SfM-MVS of Merapi Volcanic Dome and Crater Rim Change from 2012 to 2014

Christopher Gomez [1,2,*], Muhammad Anggri Setiawan [2,3], Noviyanti Listyaningrum [2,3], Sandy Budi Wibowo [4], Danang Sri Hadmoko [2,3], Wiwit Suryanto [5], Herlan Darmawan [5], Balazs Bradak [1], Rikuto Daikai [1], Sunardi Sunardi [6,7], Yudo Prasetyo [8], Annisa Joviani Astari [9], Lukman Lukman [10], Idea Wening Nurani [11,12], Moh. Dede [7], Indranova Suhendro [2,3], Franck Lavigne [12] and Mukhamad Ngainul Malawani [3,12]

1 Laboratory of Sediment Hazards and Disaster Risks, Faculty of Oceanology, Kobe University, Kobe 657-8501, Japan
2 Center for Disaster Study, Universitas Gadjah Mada, Yogyakarta 55284, Indonesia
3 Department of Environmental Geography, Faculty of Geography, Universitas Gadjah Mada, Yogyakarta 55281, Indonesia
4 Department of Geographic Information Science, Faculty of Geography, Universitas Gadjah Mada, Yogyakarta 55281, Indonesia
5 Faculty of Mathematics and Natural Sciences, Universitas Gadjah Mada, Yogyakarta 55281, Indonesia
6 Faculty of Mathematics and Natural Sciences, Universitas Padjadjaran, Sumedang 40133, Indonesia
7 Doctoral Program on Environmental Science, Postgraduate School (SPs), Universitas Padjadjaran, Bandung 40132, Indonesia
8 Department of Geodetic Engineering, Faculty of Engineering, Universitas Diponegoro, Semarang 50277, Indonesia
9 Geographic Information Science Study Program, Faculty of Social Science Education, Universitas Pendidikan Indonesia, Bandung 40154, Indonesia
10 National Research and Innovation Agency (BRIN), Cibinong 16911, Indonesia
11 Department of Development Geography, Faculty of Geography, Universitas Gadjah Mada, Yogyakarta 55281, Indonesia
12 Laboratory of Physical Geography UMR 8591, Université Paris 1 Panthéon-Sorbonne, 94320 Thiais, France
* Correspondence: christophergomez@bear.kobe-u.ac.jp

Abstract: Spatial approaches, based on the deformation measurement of volcanic domes and crater rims, is key in evaluating the activity of a volcano, such as Merapi Volcano, where associated disaster risk regularly takes lives. Within this framework, this study aims to detect localized topographic change in the summit area that has occurred concomitantly with the dome growth and explosion reported. The methodology was focused on two sets of data, one LiDAR-based dataset from 2012 and one UAV dataset from 2014. The results show that during the period 2012–2014, the crater walls were 100–120 m above the crater floor at its maximum (from the north to the east–southeast sector), while the west and north sectors present a topographic range of 40–80 m. During the period 2012–2014, the evolution of the crater rim around the dome was generally stable (no large collapse). The opening of a new vent on the surface of the dome has displaced an equivalent volume of 2.04×10^4 m^3, corresponding to a maximum -9 m ($+/-0.9$ m) vertically. The exploded material has partly fallen within the crater, increasing the accumulated loose material while leaving "hollows" where the vents are located, although the potential presence of debris inside these vents made it difficult to determine the exact size of these openings. Despite a measure of the error from the two DEMs, adding a previously published dataset shows further discrepancies, suggesting that there is also a technical need to develop point-cloud technologies for active volcanic craters.

Keywords: Merapi Volcano; Indonesia; natural hazards; disaster risk; point-cloud technology

Citation: Gomez, C.; Setiawan, M.A.; Listyaningrum, N.; Wibowo, S.B.; Hadmoko, D.S.; Suryanto, W.; Darmawan, H.; Bradak, B.; Daikai, R.; Sunardi, S.; et al. LiDAR and UAV SfM-MVS of Merapi Volcanic Dome and Crater Rim Change from 2012 to 2014. *Remote Sens.* **2022**, *14*, 5193. https://doi.org/10.3390/rs14205193

Academic Editor: Xuan Zhu

Received: 29 August 2022
Accepted: 11 October 2022
Published: 17 October 2022

1. Introduction

On stratovolcanoes, domes are a major source of hazards as they often collapse under the actions of both internal gas pressure [1] and gravity [2], creating hazardous pyroclastic-density currents [3]. Without gravitational collapses, internal gas pressure can generate explosive eruptions, eventually propelling ash and other volcanic material into the upper atmosphere. In addition, chemically stable domes can still explode as a result of phreatic and phreatomagmatic processes [4]. Even during the more quiescent phase, volcanic domes are still evolving, eventually sliding away from the top of the volcano [5] and breaking apart into "smaller pieces", generating long-runout rockfalls [6]. Environmental factors of the dome also contribute to the dome instability: for instance, precipitation contributing to hydrothermal alteration; the general movement of the volcanic structure (uplift and subsidence); the local and regional seismic activity (from Vazquez et al. after the work of McGuire [7]). However, as it was recently pointed out, despite a variety of explaining factors, the contribution of one over another remains scientifically unclear [8]. For disaster risk management and to avoid catastrophe, dome monitoring is thus essential, even during more quiescent periods.

In Central Java, Indonesia, a series of dome-collapse pyroclastic-density currents have been sweeping the flanks of Merapi Volcano during the Holocene period, although larger eruptions and sector collapses were also found in the earlier Quaternary period, known since ~360,000 BP [9,10]. The pyroclastic-density currents of the last major eruption in 2010 (VEI4: [11]) covered an area of 22.3 km^2 [12,13], in turn turning into lahars that have flooded the valleys towards Yogyakarta City [14,15]; in its aftermath, the growth of the dome has also generated rockfall hazards [6].

Consequently, the evolution of the dome has attracted the attention of scientists in different fields of research, e.g., rock geochemistry [16], gas analysis [17], numerical modeling [18], petrology [19], surface deformation [20,21], and seismology [22]. During the historical period, the dome of Merapi Volcano has been lodged into a horseshoe crater-rim, opened towards the south, directing most of the gravity collapse pyroclastic flows and rockfalls [6], locally called "*guguran*", in this same direction (Figure 1).

The present dome was born from the millennial eruption of 2010 [13], which topographically resembles a 150 m-diameter tabletop, which fractured due to phreatic explosions between 2012 and 2014 [4]. Monitoring of volcanoes and dome evolution represents significant technical challenges and risks for the personnel. Therefore, scientists have been striving to create models and simulations of dome growth and collapse [8], but field data and evidence are still essential to support those models. Focusing on the period 2012–2014, the present contribution proposes the use of high-resolution geodetic measurements from airborne LiDAR and UAV photographs for photogrammetric purposes, in order to detect topographic changes that would have occurred in the crater rim during this period of relative quiescence.

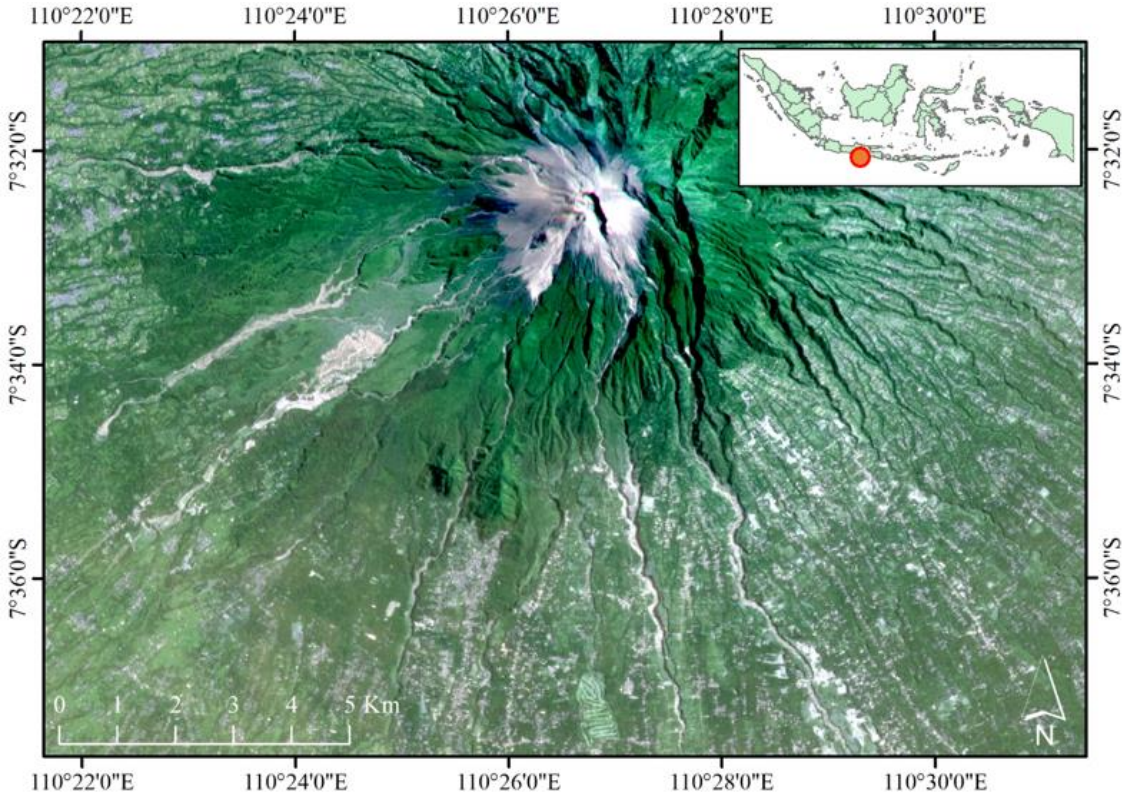

Figure 1. High-resolution (3 m) image from the PlanetScope satellite for the area of Mount Merapi and its surroundings displayed with a true color composite. Dwellings and agricultural land as close as 5 km from the dome translate into high-level disaster risk.

2. Materials and Methods

The present contribution includes two sets of data: one LiDAR-based dataset from 2012 and one UAV dataset from 2014. The 2012 dataset was derived from airborne LiDAR with a density of >5 point/m^2. The LiteMapper 5600 System was installed on a Cessna 402B Aircraft flying at an altitude of 820 m above the summit, and the photograph's airspeed was 259 km/h. The side overlap and the frontal overlap were, respectively, 40% and 60%. Concomitantly, GPS surveying for LiDAR base station was conducted at Badan Informasi Geospatial (BIG) from reference points using RTK GPS Trimble R9 with a minimum of 6 satellites. From this dataset, the 2012 data were gridded at a 1 m horizontal resolution, using the minimum vertical value (elevation) in each square-meter grid.

The 2014 dataset was built using structure from motion from 328 photographs of 3000 × 4000 pixels. The photographs were acquired on 16 October 2014 between 12:30 and 12:50 using a fix-wing UAV mounted with a Canon PowerShot S100 at a focal length of 5 mm, an exposure time of 1/1250 s, and an ISO speed of ISO-80. The photographs were integrated into the SfM–MVS (structure-from-motion multiple-view stereophotogrammetry) software Metashape Pro, commercialized by Agisoft. The process includes point-cloud reconstruction and its densification. The dense point cloud was then exported to Cloud Compare, and the point cloud was subsampled at 1 point per square meter to exactly match the point location of the LiDAR data. Using this process, the next step of comparing the two datasets limits the importance of the artifacts linked to variable point density and the horizontal distance between points. The construction and the modalities of the combination of these two datasets are as follows:

The two point clouds are then aligned in Cloud Compare (open-source software) to scale the SfM-MVS data and match it to the LiDAR point cloud using the C2C (Cloud to Cloud) algorithm, from which the distances in the x, y, and z directions are separated.

The LiDAR was thus used as the "true elevation" to calibrate the UAV photogrammetry, although errors varying based on the type of surface have been reported to vary between 18.9 cm for pavement and 25.9 cm for deciduous tree elevation [23]. Moreover, LiDAR error increases with the slope, and at Mt. Erebus, for instance, for a slope of 20 degrees, where an additional vertical error of 16 cm had to be added, locally reaching 21 cm [24]. In the present case, the authors chose to double those error values and estimate that the LiDAR was accurate to about 50 cm and that any change below this value may not be representative (although all values are reported in the article). The choice to double this value was also motivated by the possibility of sand and ash grains bouncing near the surface, increasing the potential for error.

It resulted in an RMSE (root mean square error) of 90 cm between the two point clouds when not taking into account the crater area that was known to have changed. Adding both the error from the aligned 2014 point cloud to the error assigned to the LiDAR data, the elevation error for the measurements comparing the two surfaces is about 1.4 m.

The dataset from which the authors have worked is thus made up of an orthophotograph of the summit in 2014 (Figure 2a), and two datasets of the dome in 2012 (Figure 2b) and 2014 (Figure 2c). From a visual inspection of the hill-shaded representation of the DEM, one can see the changes that have occurred on the dome (most notably the opening of vents [4]).

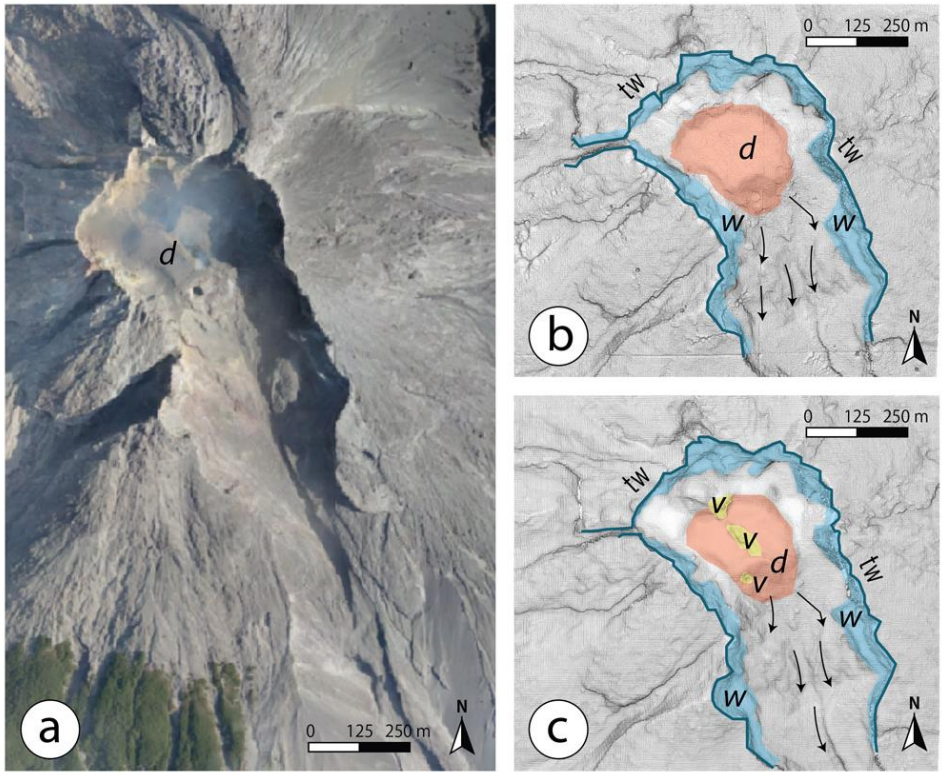

Figure 2. Dome of Merapi Volcano in 2012 and 2014: (**a**) orthophotograph constructed from UAV imagery in October 2014; (**b**) surface map of the dome in 2012 from LiDAR and (**c**) in 2014 from UAV-SfM-MVS. The captions are (d) dome in transparent red; (v) vent in transparent yellow; (tw) top of the wall and it corresponds to the blue line; (w) wall and it corresponds to the transparent blue.

3. Results

The comparison of the two topographic data is presented with first the modifications to the crater rim and the talus, and secondly, a quantification of the volume removed either from the volcanic explosions or gravitational collapses.

3.1. The Crater Rim and Its Talus

At the summit of Merapi Volcano, a horseshoe crater rim traps the dome. During the period 2012–2014, the crater walls were 100–120 m high above the crater floor at its maximum (from the north to the east–southeast sector), while the west and north sectors present a topographic range of 40–80 m (Figure 3). The crater is open to the south. During the period 2012–2014, the evolution of the crater rim around the dome was generally stable (no large collapse), although the data shows variation in the geometry of the subvertical walls around the crater rim (b–h, and k in Figure 3). The walls that spread outside of the crater rim seem to be more stable (a,l, and m in Figure 3). At the foot of the crater walls, the topography from 2012 to 2014 was stable overall, showing no major wall collapses, except in e, h, and I (Figure 3), where the floor level increased by >2 m locally. Although the walls seem to show locally large discrepancies between 2012 and 2014 (Figure 3b), the absence of significant deposits at their toes suggests that those are potential artifacts that are examined in the discussion.

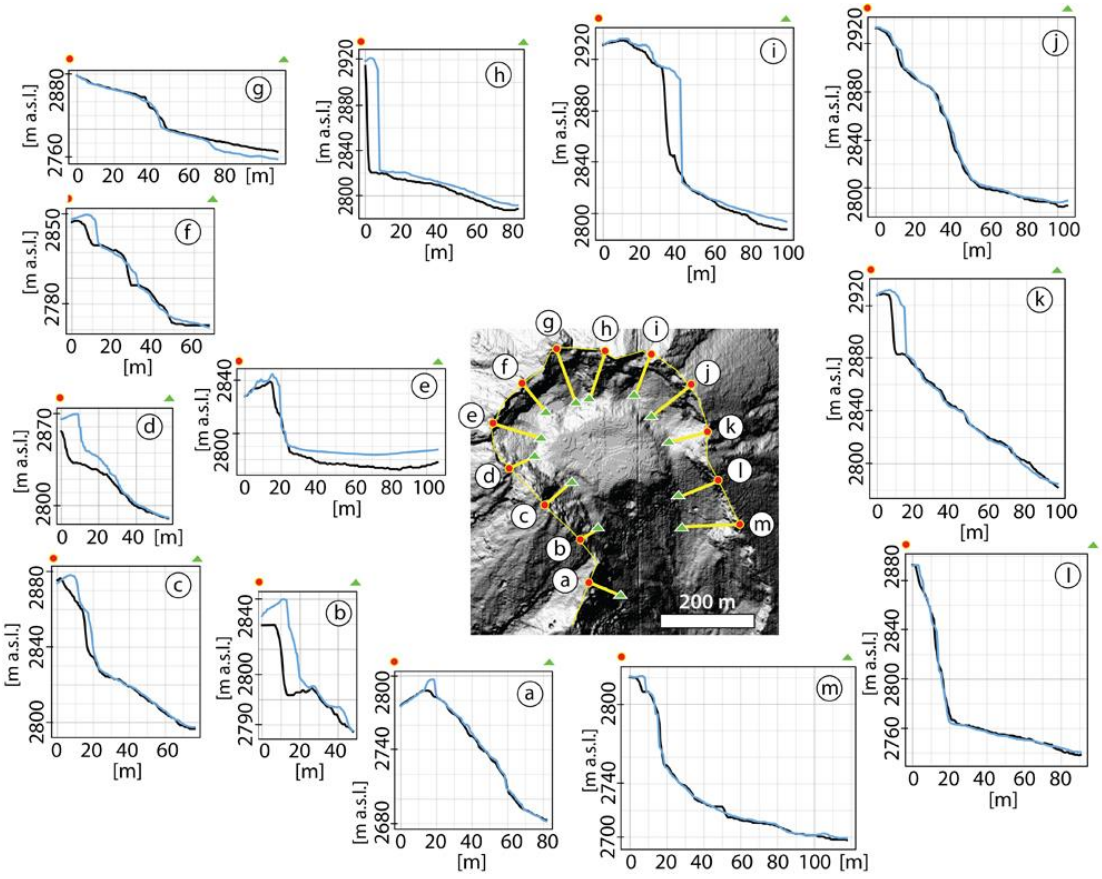

Figure 3. Cross-sections of the crater rim. The black line is the topography in 2012 as extracted from the LiDAR-DEM at 1 m horizontal resolution, and the blue line is the topography in 2014, extracted from the UAV-based photogrammetric model.

3.2. Dome's Topographic and Volumic Change with the Localized Explosions

As already reported in the literature, during the period 2012–2014, the dome locally exploded and split into a set of aligned new vents along a north–west–southeast axis. Around the dome, surface changes also occurred with an increase in elevation (Figure 4). The opening of a new vent on the surface of the dome has displaced an equivalent volume of 2.04×10^4 m^3, corresponding to a maximum -9 m ($+/-0.9$ m) vertically (location 4 in Figure 4). At the two vents generated to the north and south of the dome, the volume changes are 8.56×10^4 m^3 at location 1, 2.61×10^5 m^3 (location 2), and 4.82×10^3 m^3 at location 5 (Figure 4). The variability is mostly controlled by the visual depth of the

openings (if obstructed by debris, they appear shallower). Therefore, those values need to be considered as minimal values. Surrounding the plateau created by the dome, loose material is also displaying topographic change. It has mostly increased this time. For the period 2012–2014, the rise of material corresponds to a respective volume change of 1.88×10^4 m^3 at location 3 and 6.22×10^4 m^3 at location 8. These changes correspond to changes nearing 18 m (+/− 0.9 m) at location 1 and 11 (+/− 0.9 m) m at location 8. On top of these major topographic changes, gravitational collapses have also been observed on the crater rim (location 10) and a small portion to the south of the dome seems to have also collapsed (location 6 in Figure 4).

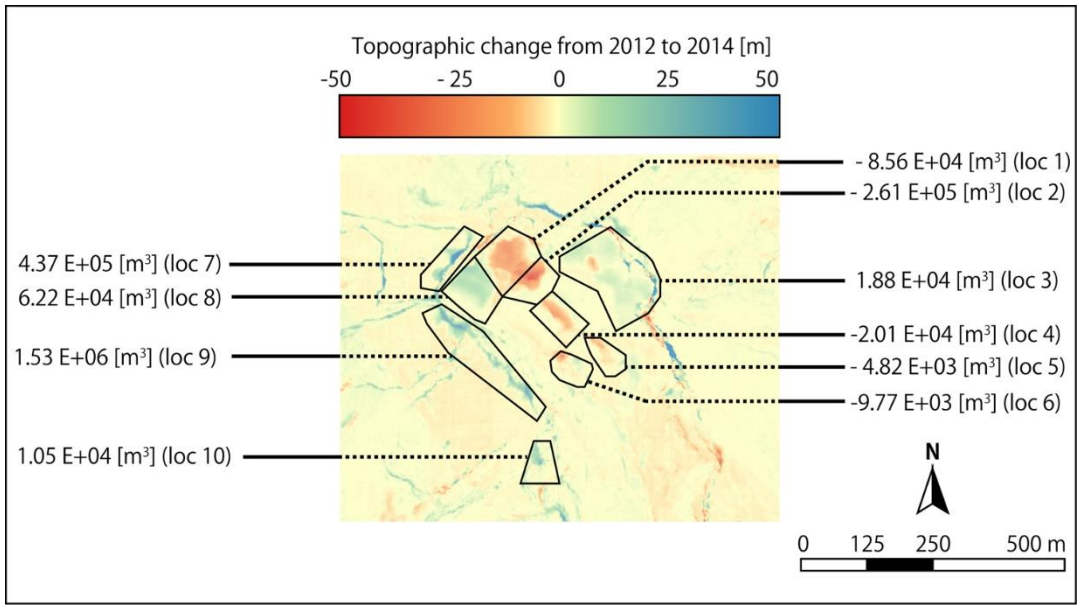

Figure 4. Topographic change from 2012 to 2014. These data show the vents opening and the "split in two" of the dome, as well as the areas between the crater rim and the dome, where the topography increased, arguably due to exploded material deposition. These changes emphasize the changes that are >2.5 m (i.e., in blue on the map), valued above the overall RMSE and the RMSE of the outside structure. This procedure may erase some of the minor variations, but it is aimed at eliminating the false positives from the dataset.

4. Discussion

This discussion is organized into two sections, with the first being an interpretation of the results and what they mean in terms of volcanic processes. Then, it follows a section that compares the data from the present contribution with a dataset from 2015, and finally we discuss the implications of the present work for hazards and disaster risk monitoring.

4.1. Surface Deformation and Interpretation

The dome of Merapi Volcano locally exploded during the period 2012–2014, creating a set of aligned vents [4], which represent an estimated volume of material of 2.01×10^4 m^3 for the central elongated vent at the top of the dome, 2.61×10^5 m^3 to the north (high-value determined by good visibility at a depth of almost 30 m below the pre-explosive surface), and one vent to the south, just shy of 1×10^4 m^3. The central elongated vent represents a topographic drop of about 9 m (Figure 5), although it is most likely that the opening could have been deeper (filled by either ejecta going back to the vent or the full depth being invisible to the SfM-MVS method due to the narrowness of the vent). The origin of these explosions is the result of pressure increase from the contact with rainwater [4] as well as probable material weakening due to hydrothermal alteration, a process that was observed at the dome summit and its surroundings at a later date [25]. Around the dome, the material in at least two locations rose topographically (Figure 5), even without having had major

wall collapses that would match this rise. If we work by analogy, the dome of 2011, which is visible between 2012 and 2014, may have grown over other extruded material in the same way that the 2017 dome climbed over the 2011 dome [25]. The exploded material may have partly escaped the space of the crater rim, but it is most likely that a large portion of it remained inside the crater, with the largest blocks traveling a shorter distance. Despite a measure of the visible volume change (Figure 4), it is difficult to link both the post-phreatic explosion holes to the deposits for the following reasons: (1) Due to decompression and deposit bulk density changing from that of the dome, the measured volume change does not reflect a material volume change; (2) Part of the material escaped the crater rim; (3) The post-explosion holes will have certainly collapsed; (3) For the deepest part of the holes, ALS or SfM-MVS may not record the real "bottom". This shows the necessity to develop a methodological framework that is more adapted to volcanic vent surveying due to the numerous complexities it holds.

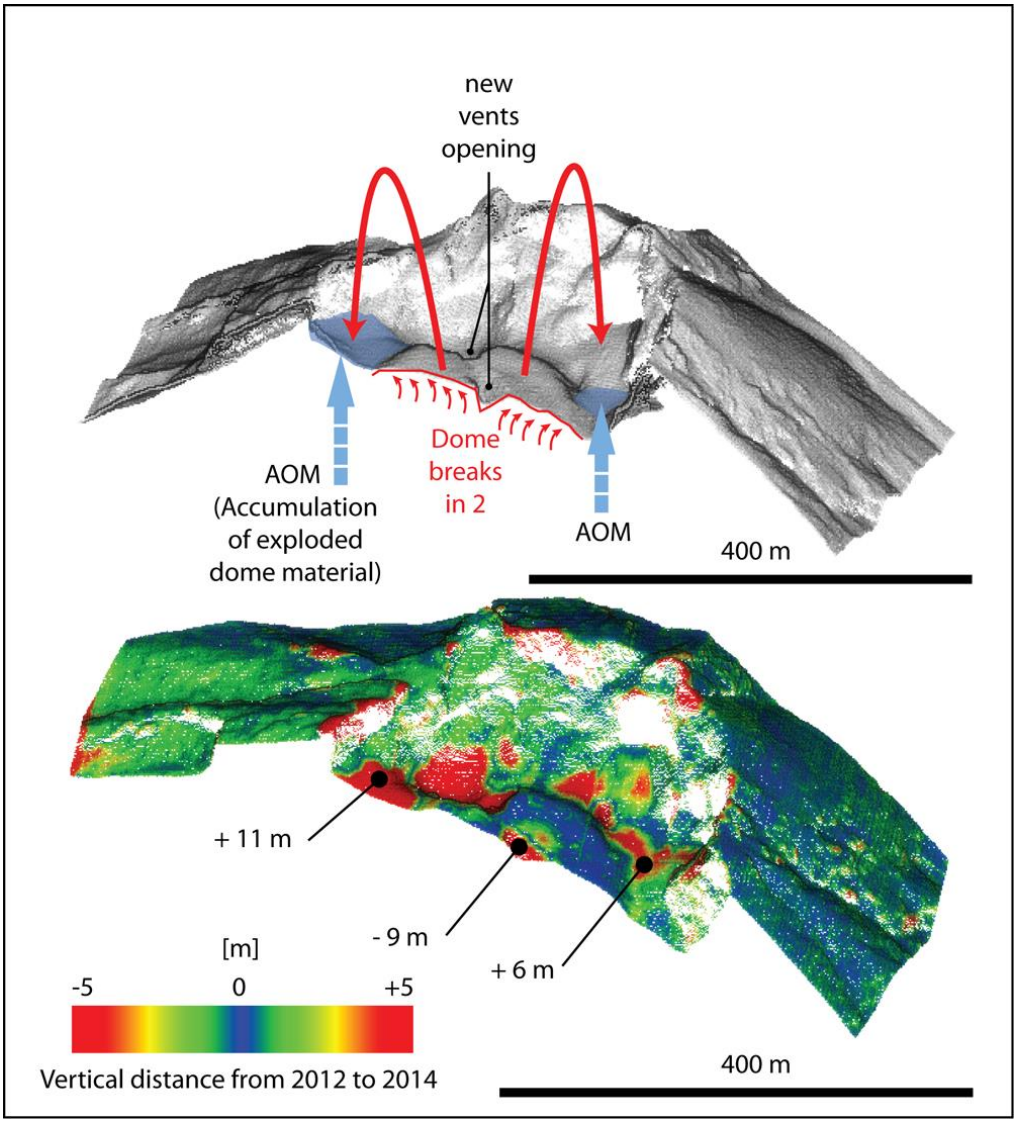

Figure 5. Interpretation figure of the deformation at the dome and near the dome.

4.2. Hazards in Quiescent Time, When the Volcano Acts as a Mountain

Even in periods when the volcano is not magmatically active [25], minor explosions and other erosion processes can also occur. In the present case, there is an accumulation of volcanic clasts within the crater and surrounding the volcanic dome. Such low-energy events can still be a hazard to mountain climbers, as has been seen at Mt. Ontake [26],

where, in 2014, around 340 individuals were located in the surrounding of the summit when it exploded, creating ballistic for which hazard maps are essential [27]. Based on the topographic change at Merapi Volcano, a large portion of the large ballistic seems to have been contained within the crater, as the topographic change from 2012 to 2014 does not show significant accumulation zones outside the crater. However, even if the material is contained within the crater and the crater is defined as a "no trespassing zone", the material produced usually ranges from fine-grain material to coarser material, and upon rainfall, the material can also be transformed into a slurry of debris and water, eventually creating lahars, such as when it did for the Ontake eruption [28]. These "small-scale" hazards can then be very pervasive because, instead of imposing a "new rhythm" on the volcano and the valley, they will be highly dependent on other factors, such as a trigger by an earthquake, or in some cases, the role of seasonal snow cladding [29]. Finally, unconsolidated material located at the summit of the volcano is a further source of hazard during long quiescent times, as it has been shown at Unzen Volcano [30], where the gullies are progressing towards the volcanic dome by regressive erosion, modifying the watershed geometries [31] and helping the release of material from the summit. In the case of a solid compact dome, breaking parts may require some "extra-effort", but if the material is already unconsolidated, it is a further pool of material that can be released on the slopes.

From a hazard perspective, small-scale explosions of a phreatic type only affect a small area, but the timing of such an explosion is extremely difficult to predict, and the fragmentation of material results in a pool of clastic sediments at the top that can then be remobilized by seasonal events (rain and snow melting) as well as longer-timescale events such as regressive erosion or eventual seismic acceleration.

5. Conclusions

The main conclusions of the present paper are that (1) during the period 2012–2014 when the dome of Merapi experienced phreatic explosions, the topography around the dome rose; (2) this rise does not seem to be related to large wall collapses, and it is likely that the exploded material accumulated in a low-topographic area; and (3) from a technical perspective, there is a need to develop UAV-imagery-acquisition methods that are fit for volcanic craters, with step walls (e.g., avoiding NADIR images), in order to reduce the error due to the lack of data; (4) volcanoes, even during quiescent time, are hazardous and for this reason, inter-eruption monitoring is essential.

Author Contributions: Conceptualization, C.G., F.L., S.B.W., D.S.H., M.N.M.; methodology, M.A.S., N.L., B.B., R.D.; resources, M.A.S., W.S., S.S., Y.P., A.J.A., L.L., I.W.N., M.D.; writing—original draft preparation, C.G.; writ-ing—review and editing, C.G., F.L., H.D., S.B.W., I.S.; funding acquisition, S.B.W., C.G. All authors have read and agreed to the published version of the manuscript.

Funding: This research was funded by Riset Kolaborasi Indonesia (RKI) number 1545/UN1/DITLIT/DitLit/PT.01.03/2022. The authors also thank two anonymous reviewers and the editor for their valuable comments to strengthen this paper. Further funding was provided at Kobe University through the IMARC international program on volcanic hazards, led by C. Gomez.

Data Availability Statement: All the data used in the present contribution can be accessed upon contacting the corresponding author.

Conflicts of Interest: The authors declare no conflict of interest.

References

1. Voight, B.; Elsworth, D. Instability and collapse of hazardous gas-pressurized lava-domes. *Geophys. Res. Lett.* **2000**, *27*, 1–4. [CrossRef]
2. Swanson, D.A.; Holcomb, R.T. Regularities in Growth of the Mount St. Helens Dacite Dome, 1980–1986. *IAVCEI Proc. Lava Flows Domes* **1990**, *2*, 3–24.

3. Loughlin, S.C.; Calder, E.S.; Clarke, A.; Cole, P.D.; Luckett, R.; Mangan, M.T.; Pyle, D.M.; Sparks, R.S.J.; Voight, B.; Watts, R.B. Pyroclastic flows and surges generated by the 25 June 1997 dome collapse, Soufriere Hills Volcano, Montserrat. In *The Eruption of Soufriere Hills Volcano, Montserrat, from 1995 to 1999*; Druit, T.H., Kokelaar, B.P., Eds.; Geological Society: London, UK, 1990; Volume 21, pp. 129–209.
4. Darmawan, H.; Walter, T.R.; Troll, V.R.; Budi-Santoso, A. Structural weakening of the Merapi dome identified by drone photogrammetry after the 2010 eruption. *Nat. Hazards Earth Syst. Sci.* **2018**, *18*, 3267–3281. [CrossRef]
5. Gomez, C.; Allouis, C.; Lissak, N.; Hotta, N.; Shinohara, Y.; Hadmokok, D.S.; Vilimek, V.; Wassmer, P.; Lavigne, F.; Setiawan, A.; et al. *High-Reolustion Point-Cloud for Landslides in the 21st Century: From Data Acquisition to New Processing Concepts, In Understanding and Reducing Landslide Disaster Risk*; Arbanas, Z., Ed.; Springer Nature: Cham, Switzerland, 2021; Volume 6, pp. 199–213.
6. Darmawan, H.; Yuliantoro, P.; Rakhman, A.; Santoso, A.B.; Humaida, H.; Suryanto, W. Dynamic velocity and seismic characteristics of gravitational rockfalls at the Merapi lava dome. *J. Volcanol. Geotherm. Res.* **2020**, *404*, 107010. [CrossRef]
7. Vazquez, R.; Macias, J.L.; Alcala-Reygosa, J.; Arce, J.L.; Jimenez-Haro, A.; Fernandez, S.; Carlon, T.; Saucedo, R.; Sanchez-Nunez, J.M. Numerical modeling and hazard implications of landslides at the Ardillas Volcanic Dome (Tacana Volcanic Complex, Mexico-Guatemala). *Nat. Hazards* **2022**, *113*, 1305–1333. [CrossRef]
8. Kelfoun, K.; Santoso, A.B.; Latchimy, T.; Bontemps, M.; Nurdienm, I.; Beauducel, F.; Fahmi, A.; Putra, R.; Dahamna, N.; Laurin, A.; et al. Growth and collapse of the 2018–2019 lava dome of Merapi Volcano. *Bull. Volcanol.* **2021**, *83*, 8. [CrossRef]
9. Gomez, C.; Janin, M.; Lavigne, F.; Gertisser, R.; Charbonnier, S.; Lahitte, P.; Hadmoko, D.S.; Fort, M.; Wassmer, P.; Degroot, V.; et al. Borobudur, a basin under volcanic influence: 361,000 years BP to present. *J. Volcanol. Geotherm. Res.* **2010**, *196*, 245–264. [CrossRef]
10. Newhall, C.G.; Bronto, S.; Alloway, B.; Banks, N.G.; Bahar, I.; del Marmol, M.A.; Hadisantono, R.D.; Holcomb, R.T.; McGeehin, J.; Miksic, J.N.; et al. 10,000 years of explosive eruptions of Merapi Volcano, Central Java: Archeological and modern implications. *J. Volcnaol. Geotherm. Res.* **2000**, *100*, 9–50. [CrossRef]
11. Surono; Jousset, P.; Pallister, J.; Boichu, M.; Buongiorno, M.; Budisantoso, A.; Costa, F.; Andreastuti, S.; Prata, F.; Schneider, D.; et al. The 2010 explosive eruption of Java's Merapi volcano—A '100-year' event. *J. Volcanol. Geotherm. Res.* **2012**, *241–242*, 121–135. [CrossRef]
12. Charbonnier, S.J.; Germa, A.; Connor, C.B.; Gertisser, R.; Preece, K.; Komorowski, J.-C.; Lavigne, F.; Dixon, T.; Connor, L. Evaluation of the impact of the 2010 pyroclastic density currents at Merapi volcano from high-resolution satellite imagery, field investigations and numerical simulations. *J. Volcanol. Geotherm. Res.* **2013**, *261*, 295–315. [CrossRef]
13. De Belizal, E.; Lavigne, F.; Robin, A.K.; Sri Hadmoko, D.; Cholik, N.; Thouret, J.C.; Sawudi, D.S.; Muzani, M.; Sartohadi, J.; Vidal, C. Rain-triggered lahars following the 2010 eruption of Merapi volcano, Indonesia: A major risk. *Volcanol. Geotherm. Res.* **2013**, *261*, 330–347. [CrossRef]
14. Komorowski, J.-C.; Jenkins, S.; Baxter, P.J.; Picquout, A.; Lavigne, F.; Charbonnier, S.; Gertisser, R.; Preece, K.; Cholik, N.; Budi-Santo, A.; et al. Paroxysmal dome explosion during the Merapi 2010 eruption: Processes and facies relationships of associated high-energy pyroclastic density currents. *J. Volcanol. Geotherm. Res.* **2013**, *261*, 260–294. [CrossRef]
15. Sri Hadmoko, D.; de Belizal, E.; Mutaqin, B.W.; Dipayana, G.A.; Marfai, M.A.; Lavigne, F.; Sartohdai, J.; Worosuprojo, S.; Starheim, C.A.; Gomez, C. Post-eruptive lahars at Kali Putih following the 2010 eruption of Merapi Volcano, Indonesia: Occurrences and impacts. *Nat. Hazards* **2018**, *94*, 419–444. [CrossRef]
16. Allard, P. Proportions des isotopes 13 C et 12 C du carbone émis à haute température par un dome andésitique en cours de croissance; Le Merapi (Indonésie)—Proportions of C-13 and C-12 isotopes of carbon emitted at high temperature by an andesitic dome during growth; Merapi, Indonesia. *C. R. Acad. Sci. Série D* **1980**, *291*, 613–616.
17. Le Guern, F.; Gerlach, T.M.; Nohl, A. Field gas chromatograph analyses of gases from a glowing dome at Merapi Volcano, Java, Indonesia, 1977, 1978, 1979. *J. Volcanol. Geotherm. Res.* **1982**, *14*, 223–245. [CrossRef]
18. Kelfoun, K. Processus de Croissance et de Déstabilisation des Dômes de lave du Volcan Merapi (Java Centrale, Indonésie). Modélisations Numériques des Dômes, Dynamique des Ecoulements Pyroclastiques Associés et Surveillance par Stéréophotogrammétrie. Ph.D. Thesis, Univ. Blaise Pascal Clermont-Ferrand II, Aubière, France, 1999.
19. Clocchiatti, R.; Joron, J.-L.; Kerinec, F.; Treuil, M. Quelques données préliminaires sur la lave du dome actuel du volcan Merapi (Java, Indonésie) et sur ses enclaves—Preliminary data on lava from the present dome of the volcano Merapi (Java, Indonesia) and on its xenoliths. *C. R. Acad. Sci. Série 2* **1982**, *295*, 817–822.
20. Voight, B.; Young, K.D.; Hidayat, D. Deformation and seismic precursors to dome-collapse and fountain-collapse nuées ardentes at Merapi Volcano, Java, Indonesia, 1994–1998. *J. Volcanol. Geotherm. Res.* **2000**, *100*, 261–287. [CrossRef]
21. Young, K.D.; Voight, B. Ground deformation at Merapi Volcano, Java, Indonesia: Distance changes, June 1988–October 1995. *J. Volcanol. Geotherm. Res.* **2000**, *100*, 233–259. [CrossRef]
22. Brodscholl, A.; Kirbani, S.B.; Voight, B. Sequential dome-collapse nuées ardentes analyzed from broadband seismic data, Merapi Volcano, Indonesia. *J. Volcanol. Geotherm. Res.* **2000**, *100*, 363–369. [CrossRef]
23. Hodgson, M.E.; Bresnahan, P. Accuracy of Airborne Lidar-Derived Elevation: Empirical Assessment and Error Budget. *Photogram. Eng. Remote Sens.* **2004**, *70*, 331–339. [CrossRef]
24. Csatho, B.; Schenck, T.; Kyle, P.; Wilson, T.; Krabill, W.B. Airborne laser swath mapping of the summit of Erebus volcano, Antarctica: Applications to geological mapping of a volcano. *J. Volcanol. Geotherm. Res.* **2008**, *177*, 531–548. [CrossRef]

25. Darmawan, H.; Troll, V.R.; Walter, T.R.; Deegan, F.M.; Geiger, H.; Heap, M.J.; Seraphine, N.; Harris, C.; Humaida, H.; Muller, D. Hidden mechanical weaknesses within lava domes provided by buried high-porosity hydrothermal alteration zones. *Sci. Rep.* **2022**, *12*, 3202. [CrossRef] [PubMed]
26. Tsunematsu, K.; Ishimine, Y.; Kaneko, T.; Yoshimoto, M.; Fujii, T.; Yamaoka, K. Estimation of ballistic block landing energy during 2014 Mount Ontake eruption. *Earth Planets Space* **2016**, *68*, 88. [CrossRef]
27. Fitzgerald, R.H.; Tsunematsu, K.; Kennedy, B.M.; Breard, E.C.P.; Lube, G.; Wilson, T.M.; Jolly, A.D.; Pawson, J.; Rosenberg, M.D.; Cronin, S.J. The application of a calibrated 3D ballistic trajectory model to ballistic hazard assessments at Upper Te Maari, Tongariro. *J. Volcanol. Geotherm. Res.* **2014**, *286*, 248–262. [CrossRef]
28. Kataoka, K.S.; Matsumoto, T.; Saito, T.; Nagahashi, Y.; Iyobe, T. Suspended sediment transport diversity in river catchments following the 2014 phreatic eruption at Ontake Volcano, Japan. *Earth Planets Space* **2019**, *71*, 15. [CrossRef]
29. Kataoka, K.S.; Matusmoto, T.; Saito, T.; Kawashima, K.; Nagahashi, Y.; Iyobe, T.; Sasaki, A.; Suzuki, K. Lahar characteristics as a function of triggering mechanism at a seasonally snow-clad volcano: Contrasting lahars following the 2014 phreatic eruption of Ontake Volcano, Japan. *Earth Planets Space* **2018**, *70*, 113. [CrossRef]
30. Tsunetaka, H.; Shinohara, Y.; Hotta, N.; Gomez, C.; Sakai, Y. Multi-decadal changes in the relationships between rainfall characteristics and debris-flow occurrences in response to gully evolution after the 1990-1995 Mount Unzen eruptions. *Earth Surf. Process. Landf.* **2021**, *46*, 2141–2162. [CrossRef]
31. Gomez, C.; Shinohara, Y.; Tsunetaka, H.; Hotta, N.; Bradak, B.; Sakai, Y. Twenty-Five Years of Geomorphological Evolution in the Gokurakudani Gully (Unzen Volcano): Topography, Subsurface Geophysics and Sediment Analysis. *Geosciences* **2021**, *11*, 457. [CrossRef]